Acta Geochim (2025) 44:731–739
https://doi.org/10.1007/s11631-024-00752-9

ORIGINAL ARTICLE

Stable strontium isotope fractionation during crystal-melt separation in granitic magma evolution

Xuqi Chen[1] · Gengxin Deng[1] · Dingsheng Jiang[1] · Xiaoyun Nan[1] · Fang Huang[1,2]

Received: 2 December 2024 / Revised: 20 December 2024 / Accepted: 25 December 2024 / Published online: 8 January 2025

Abstract Stable Sr isotopic composition ($\delta^{88/86}$Sr) can be used to study magmatic processes, but their fractionation mechanism during magmatic evolution remains unclear. To understand the fractionation behaviors of the stable Sr isotopes during magmatism, we report the $\delta^{88/86}$Sr values of the Huili granitic pluton, which was subjected to intensive crystal-melt separation. The Huili pluton consists of K-feldspar granite and more evolved albite granite, and the albite granite exhibits significantly higher $\delta^{88/86}$Sr values (+0.36‰ to +0.52‰) than that of K-feldspar granite (+0.11‰ to +0.25‰). K-feldspar, which contributes most of the Sr budget of the K-feldspar granite, has slightly lower $\delta^{88/86}$Sr values (−0.01‰ to +0.17‰) than the whole rock. The $\delta^{88/86}$Sr variation of the Huili granites can be explained by separation of melt from K-feldspar-dominated crystals, because crystallization of K-feldspar can result in heavy Sr isotopic composition of the extracted interstitial melt. Stable Sr and Ba isotopic ratios in the Huili granites are highly coupled toward the heavy direction, reflecting their similar element partitioning and isotope fractionation behaviors between the crystalline K-feldspar and melt. This study indicates that melt extraction plays a key role in granitic magma evolution.

Keywords Stable Sr isotopes · Granite · Crystal-melt separation · Isotope fractionation

1 Introduction

As an alkaline earth metal element, Sr^{2+} has an ionic radius similar to Ca^{2+} (Shannon 1976), and it thus can replace Ca^{2+} in the crystal lattice of many minerals. In basaltic magma, strontium usually behaves as an incompatible element, which is preferentially enriched in the melt during partial melting and crystallization (Hofmann 1988). Therefore, Sr is more enriched in the oceanic and continental crust relative to the mantle (Hofmann 1988; Rudnick and Fountain 1995). In felsic magma, because Sr is compatible in plagioclase, K-feldspar, apatite, and other accessory minerals, Sr contents in evolved magmas decrease with magma differentiation (Blundy and Wood 1991; Icenhower and London 1996; Prowatke and Klemme 2006; Arzilli et al. 2018). Sr is also a large ion lithophile element (LILE) and fluid-mobile element (Keppler 2017; Iveson et al. 2019). Because of its unique properties, Sr has been widely used to trace mineral crystallization and fluid activity during magmatic processes.

Sr has four stable isotopes: ^{84}Sr (0.56%), ^{86}Sr (9.86%), ^{87}Sr (7.00%), and ^{88}Sr (82.58%) (Meija et al. 2016). In addition to geochronological applications combined with ^{87}Rb/^{86}Sr (e.g., Faure 1986), the radiogenic Sr isotope ratio (^{87}Sr/^{86}Sr) is a common tracer to indicate the sources of terrestrial materials. In the last decades, stable Sr isotopic composition, defined as $\delta^{88/86}\mathrm{Sr} = [(^{88}\mathrm{Sr}/^{86}\mathrm{Sr})_{\mathrm{sample}}/(^{88}\mathrm{Sr}/^{86}\mathrm{Sr})_{\mathrm{SRM987}} - 1] \times 1000$ ‰, has been applied in the studies on cosmochemistry (e.g., Moynier et al 2010; Bekaert et al. 2021) and surficial processes (e.g., Andrews and Jacobson 2017; Paytan et al. 2021). Sr isotope systematics have a unique advantage because they can not only

Supplementary Information The online version contains supplementary material available at https://doi.org/10.1007/s11631-024-00752-9.

✉ Fang Huang
fhuang@ustc.edu.cn

[1] State Key Laboratory of Lithospheric and Environmental Coevolution, School of Earth and Space Sciences, University of Science and Technology of China, Hefei 230026, China

[2] Center for Excellence in Comparative Planetology of CAS, University of Science and Technology of China, Hefei 230026, China

indicate the Sr source using $^{87}Sr/^{86}Sr$ but also constrain the geochemical process using $^{88/86}Sr$ (e.g., Ohno et al. 2008; Andrews et al. 2016; Shao et al. 2021). Therefore, combining $^{87}Sr/^{86}Sr$ with $^{88}Sr/^{86}Sr$, the Sr isotopes can provide useful insights into the study of magmatism. However, the fractionation behaviors of stable Sr isotopes during magmatic processes are not clear, which hinder further applications of Sr isotopes.

Because highly evolved granites usually record complex differentiation processes of granitic magmatic system (e.g., Michaud and Pichavant 2020; Fan et al. 2022), they provide a good opportunity to study the fractionation behaviors of the stable Sr isotopes during granitic magma differentiation. Previous studies observed significant $\delta^{88/86}Sr$ variation (−0.19‰ to 0.446‰) of felsic igneous rocks (e.g., Charlier et al. 2012, 2017), and part of them was attributed to crystallization of plagioclase which is preferentially enriched in heavy Sr isotopes (Charlier et al. 2012; Klaver et al. 2020). However, during the granitic magmatic differentiation, the effect of crystallization of other Sr-bearing minerals on stable Sr isotopes is still not well understood.

This study presents stable Sr isotopic compositions of the well characterized highly evolved Huili granitic pluton. It locates in the Jiaobei Terrane in the North China Craton, which is composed of two groups of K-feldspar granites and one group of albite granite. Because the Huili granites mainly experienced K-feldspar-dominating crystal-melt separation process (Li et al. 2017; Deng et al. 2021), we selected the Huili granites to investigate the fractionation behavior for stable Sr isotopes during crystal-melt separation. Our study finds that the crystal-melt separation dominated by K-feldspar has a significant effect on the stable Sr isotopic composition of the granitic magma.

2 Materials and methods

2.1 Geological background and samples

The irregular Paleoproterozoic Huili granitic pluton, which is located in the northeastern Jiaobei Terrane in the North China Craton (Fig. S1a), is approximately 10 km long and 3 km wide. The pluton is slightly foliated, intruding into the highly deformed quartz-feldspar gneiss of the Jingshan Group (Fig. S1b). According to the petrographic and geochemical characteristics, the 21 Huili granite samples in this study can be divided into three groups: groups I and II are coarse- to medium-grained two-mica granites with K-feldspar phenocrysts, and group III is medium- to fine-grained muscovite granite with albite phenocrysts (Li et al. 2017). Groups I and II granites mainly consist of K-feldspar (~40%), quartz (~35%), plagioclase (~22%) and minor amounts of biotite and muscovite, and group III granite mainly consists of plagioclase (~45%), quartz (35%), K-feldspar (~17%) and minor muscovite. Observation at the thin sections indicates no apparent mineral alteration in most samples, and only slight alteration of plagioclase and biotite grains in a few samples. Zircon U–Pb dating of the three groups of granites show a same crystallization age of ca. 1.86 Ga, and the $\varepsilon_{Nd}(t)$ values of all samples are ranging from −4.0 to −6.2 with the two-stage Nd model ages ranging from 2.67 to 2.85 Ga (Li et al. 2017). Barium isotopic composition indicates that the Huili granitic magma experienced crystal accumulation and repacking during crystal-melt separation (Deng et al. 2021).

The Huili granites are silica-saturated (SiO_2 = 71.68–74.79 wt%), alkali enriched ($K_2O + Na_2O$ = 7.49–9.30 wt.%), slightly peraluminous (A/NK = 1.15–1.3 and A/CNK = 1.06–1.31), and they have low $Fe_2O_3^t$, TiO_2, and MgO contents ($Fe_2O_3^t + TiO_2 + MgO$ = 0.78–2.28 wt%). The major and trace element compositions of groups I and II K-feldspar granites are similar except for the different CaO contents. Group III albite granite has higher SiO_2 and Al_2O_3 contents and lower Fe_2O_3, TiO_2, and CaO contents, indicating that the group III albite granite experienced higher degrees of magma evolution (Li et al. 2017; Fig. S2). In addition to the 21 whole-rock samples, we selected 6 K-feldspar and 1 plagioclase samples from group I K-feldspar granite, 3 K-feldspar samples from group II K-feldspar granite, and 1 K-feldspar sample from group III albite granite for Sr isotope analyses.

2.2 Analytical methods

Sr isotope analyses for both whole-rock and mineral samples were carried out in the State Key Laboratory of Lithospheric and Environmental Coevolution at the University of Science and Technology of China (USTC), Hefei, China. The rocks were crushed into small grains with diameter ~ 1 mm, and then subjected to the separation procedure for minerals including magnetic separation, manual extraction, and density separation (Deng et al. 2021). Ten K-feldspar and one plagioclase samples (each sample contains tens of mineral grains) were selected from the three groups of the Huili granites. To ensure the purity of the minerals, we used a Raman spectroscopy (LabRAM HR Evolution, HORIBA Jobin Yvon, France) to identify the specific mineral types of the selected feldspar grains.

Sample digestion and Sr purification were performed in an ISO class 6 clean room. Whole-rock powders and mineral grains containing approximately 0.8–2 μg Sr were digested by a 1:3 mixture of concentrated HNO_3 and HF at 125℃ for more than 24 h. After drying down the samples, aqua regia and HCl were successively used to breakdown fluorides, and then the digested samples were dissolved in 1 mL of 2.5 mol/L HCl. The purification for Sr was applied

through a two-column procedure using a cation exchange resin (AG50W-X12, 200–400 mesh; Bio-Rad®, USA). Sr was separated from major elements and Rb by eluting with 2.5 mol/L HCl and 4 mol/L HCl on the first column, and then separated from rare earth elements (REEs) by eluting with 2 mol/L HNO_3 on the second column (Chen et al. 2022). The purified Sr solutions were evaporated to dryness, and then dissolved and diluted to ~ 200 ng/g with 2% (m/m) HNO_3 for Sr isotope analyses. The total procedure blanks were less than 0.3 ng. To rigorously evaluate the recovery rate of Sr and potential Sr isotope fractionation during the chromatographic purification, the 1 mL eluents before and after the "Sr-collection" were collected to examine whether the elution curve drifted, and comparative experiments of adding double-spike before and after column purification for seven geological reference materials (i.e., five igneous rocks and 2 soils) were conducted. The results of the samples spiked before column purification are consistent with the those of the samples spiked after column purification (Fig. S3), indicating a high recovery rate of Sr and negligible Sr isotope fractionation during our chromatographic purification procedure. Therefore, the whole-rock and mineral samples in this study were all spiked after column purification.

Sr isotope analysis was performed by a multiple-collector inductively coupled plasma-mass spectrometry (MC-ICP-MS) (Neptune Plus, Thermo Fisher Scientific®, Germany). Sample solution was introduced using nickel Jet and H cones (Thermo Fisher Scientific®), an ESI PFA nebulizer, and a quartz dual cyclonic spray chamber. The Sr isotope measurement was performed in low resolution mode (> 10 V for ^{88}Sr while Sr ~ 200 ng/g). Faraday cups L2, C, H1, and H2 were used to collect ^{84}Sr, ^{86}Sr, ^{87}Sr, and ^{88}Sr, respectively. L3 and L1 were also used to monitor ^{83}Kr and ^{85}Rb for isobaric interference corrections assuming similar instrumental fractionation factors of Kr, Rb, and Sr, and natural isotope abundances of Kr and Rb. Rb was well removed after the two-column purification, and most of the purified samples had $^{85}Rb/^{86}Sr$ less than 0.0004. Even Rb isotopes may fractionate during chromatographic purification, its effect on the correction is negligible. In addition, the Kr content in the Ar gas was also low with ^{83}Kr less than 0.1 mV. Therefore, the corrections of isobaric interferences were effective.

Each sample needs a two-step measurement to successively obtain $^{87}Sr/^{86}Sr$ and $\delta^{88/86}Sr$ values. In the first step without double-spike, we used $^{86}Sr/^{88}Sr = 0.1194$ (Nier 1938) and the exponential law to correct instrument mass bias for $^{87}Sr/^{86}Sr$. In the second step, an ^{84}Sr-^{87}Sr double-spike ($^{84}Sr = 52.1\%$, $^{86}Sr = 2.7\%$, $^{87}Sr = 32.4\%$, $^{88}Sr = 12.8\%$) was added into the sample solution ($Sr_{DS}/Sr_{sample} \sim 0.7$) for mass bias calibration. Both $^{87}Sr/^{86}Sr$ and $\delta^{88/86}Sr$ for each sample were measured at least twice, and for each time, the data were acquired in one block of 40 cycles with integration time of 4.194 s. To evaluate the accuracy and precision of Sr isotope analysis, three USGS reference materials (i.e., G-2, AGV-2, and BHVO-2) were digested, purified, and measured together with the samples; and in the measurement sequence, the isotopic standard SRM 987 and two pure Sr solutions (i.e., USTC-Sr and GB-Sr; Chen et al. 2022) were alternately measured with the samples to ensure the stability of the instrument operation. Our $\delta^{88/86}Sr$ results for the USGS reference materials (Table S1) are 0.33‰ ± 0.03‰ (2SD, n = 3) for G-2, 0.26‰ ± 0.02‰ (2SD, n = 4) for AGV-2, and 0.26 ± 0.02‰ (2SD, n = 2) for BHVO-2, which are consistent with the literature data (e.g., Liu et al. 2012; Chen et al. 2022 and references therein), indicating the reliability of our measurement. Combined with the results of the pure Sr solutions and the geological reference materials (Fig. S3, S4), the long-term precision for $\delta^{88/86}Sr$ analysis is better than 0.03‰ (2SD).

3 Results

The Sr isotope data of whole-rock and mineral samples of the Huili granites and reference materials are shown in Table S1. For the Huili granites, replicate analyses for five whole-rock samples and two mineral samples obtain $^{87}Sr/^{86}Sr$ values different by 0.000071 to 0.005170, and the $^{87}Sr/^{86}Sr$ values for the whole-rock samples are also slightly different from the published data (Li et al. 2017). Considering the old age (ca. 1.86 Ga) and the high Rb/Sr ratios (1.0–6.9) for the Huili granites (Li et al. 2017), the slight heterogeneity of the Rb/Sr for whole-rock powders or mineral grains can result in significant variation in $^{87}Sr/^{86}Sr$. In contrast, the seven groups of replicates show consistent $\delta^{88/86}Sr$ with two standard errors ≤ 0.03‰, indicating that the heterogeneity of $^{87}Sr/^{86}Sr$ does not affect the measurement of $\delta^{88/86}Sr$, which is homogeneous at the hand specimen scale.

The whole-rock $\delta^{88/86}Sr$ values of the Huili granites vary significantly from 0.11‰ to 0.52‰. The two groups of K-feldspar granites have similar and small $\delta^{88/86}Sr$ variation: the $\delta^{88/86}Sr$ values of group I granite are from 0.11‰ to 0.25‰, while that of group II granite are from 0.17‰ to 0.22‰. In contrast, group III albite granite is significantly enriched in heavy Sr isotopes (Fig. 1), with $\delta^{88/86}Sr$ values ranging from 0.36‰ to 0.52‰. The K-feldspar samples show a narrow range of $\delta^{88/86}Sr$ values (−0.01‰ to 0.17‰), which is slightly lower than the relative whole-rock samples. The two replicates of plagioclase have high $\delta^{88/86}Sr$ values with an average of 0.53‰.

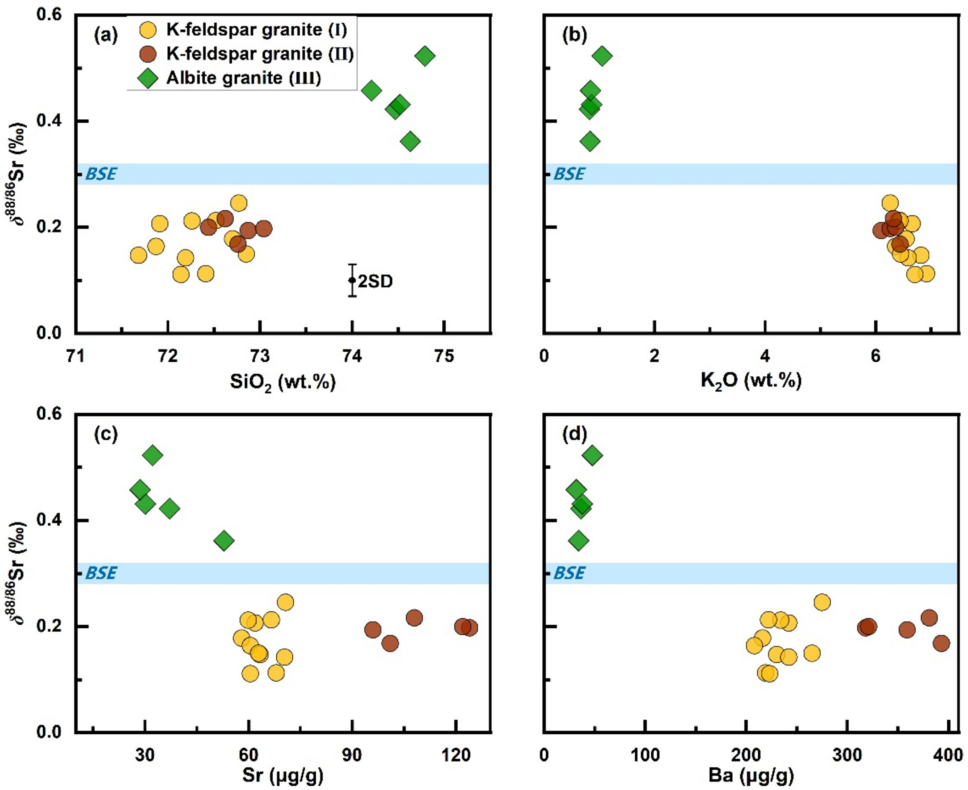

Fig. 1 Correlations of whole-rock stable Sr isotopic compositions and (**a**) SiO_2 contents, (**b**) K_2O contents, (**c**) Sr contents, and (**d**) Ba contents of Huili granites (Li et al. 2017). The error bar represents two standard deviations based on the long-term external precision for $\delta^{88/86}Sr$ (2SD = ±0.03‰). The blue stripes represent the average $\delta^{88/86}Sr$ (0.30‰ ± 0.02‰, 2SD; Amsellem et al. 2018) of the Bulk Silica Earth (BSE)

4 Discussion

4.1 The effect of weathering, assimilation, and magmatic-fluid interaction

The whole-rock $\delta^{88/86}Sr$ variation for the Huili granites is up to 0.41‰, showing significant difference between two groups of K-feldspar granites and group III albite granite. Because Sr isotopes may be fractionated during multiple processes such as surface weathering, assimilation, crystallization, and magmatic-fluid interaction, we need to carefully consider the reason for $\delta^{88/86}Sr$ variation in the Huili granites.

Although slight alteration of plagioclase and biotite grains were observed in the thin sections of a few samples, such slight alterations have a negligible effect on whole-rock compositions, because elements such as Na and K which are easily migrated during chemical weathering of this samples are consistent with the unaltered samples. Groups I and III granites have chemical index of alteration (CIA) (from 51.5 to 54.5) within the range of fresh granites (i.e., from 45 to 55) (Nesbitt and Young 1982), indicating trivial effect of chemical weathering. Group II K-feldspar granite shows slightly higher CIA from 55.2 to 56.7, but it obtains $\delta^{88/86}Sr$ values consistent with those of group I K-feldspar granite without correlation with CIA (Fig. 2a). Therefore, chemical weathering should not produce notable whole-rock variation in $\delta^{88/86}Sr$. Moreover, the lack of correlation between whole-rock $\delta^{88/86}Sr$ and $\varepsilon_{Nd}(t)$ suggests that wall rock assimilation or heterogeneous source cannot account for the stable Sr isotope fractionation (Fig. 2b). All samples have Nb/Ta greater than 5 (Fig. 2c) and Zr/Hf greater than 26 (Li et al. 2017), indicating that magmatic-fluid interaction is less likely to occur during the formation of the Huili granites (Bau et al. 1996; Ballouard et al. 2016). The lack of correlation between $\delta^{88/86}Sr$ and Nb/Ta (Fig. 2c) also indicates that the $\delta^{88/86}Sr$ variation cannot be attributed to fluid activity.

4.2 The effect of crystal-melt separation dominated by K-feldspar

Petrologic, mineralogical, and geochemical evidence reveal that the Huili granites mainly experienced a crystal-melt separation process controlled by K-feldspar. Observations of the thin sections of the K-feldspar granite reveal some textural features suggesting that K-feldspar was the main crystalline mineral during early crystallization, including concentration of mostly interlocking euhedral or subhedral K-feldspar phenocrysts with interstitial finer-grained aggregates of anhedral quartz and plagioclase, coarse grained concentrations of K-feldspar, and local synneusis K-feldspar clusters (Deng et al. 2021). Compared with groups I and II K-feldspar granites, group III albite granite has significantly higher Na_2O contents, lower K_2O

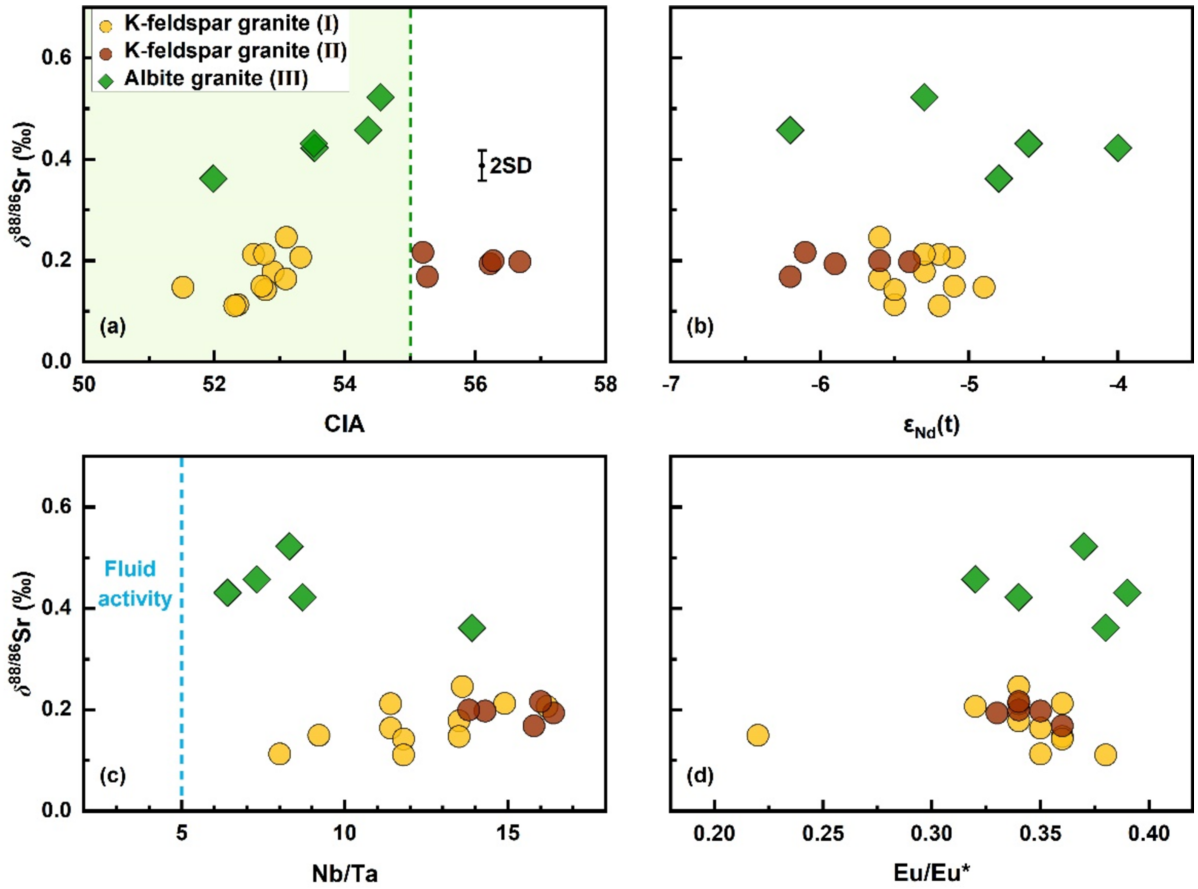

Fig. 2 Correlations of whole-rock stable Sr isotopic compositions and (**a**) CIA, (**b**) $\varepsilon_{Nd}(t)$, (**c**) Nb/Ta, and (**d**) Eu/Eu^* of Huili granites (Li et al. 2017). The error bar represents two standard deviations based on the long-term external precision for $\delta^{88/86}Sr$ (2SD = ± 0.03‰). The green shade in (**a**) represents fresh granites with CIA ranging from 45 to 55 (Nesbitt and Young 1982)

contents and K-feldspar compatible elements (e.g., Rb, Ba, Pb, and Cs) (Li et al. 2017). A reasonable explanation for the formation of the three groups of Huili granites is that the K-rich magma derived from remelting of ancient crust first experienced fractional crystallization dominated by K-feldspar to form a "crystal mush" composed of K-rich minerals and Na-rich liquid interstitial melt. Subsequently, part of the interstitial melt was extracted to form albite granite which can be represented by group III albite granite, and the residual crystal mush cooled to form K-feldspar granite which can be represented by groups I and II granites (Li et al. 2017). The coexisting minerals in the K-feldspar granite are not in Ba isotope equilibrium, indicating a complex process including crystal accumulation and repacking during crystal-melt separation (Deng et al. 2021). The SiO_2, Na_2O, K_2O, Sr, and Ba contents are distinct between K-feldspar granites and group III albite granite (Fig. S2), and the $\delta^{88/86}Sr$ also show obvious "compositional gaps" (Bachmann and Huber 2016) between the two kinds of granites (Fig. 1) due to the melt-mineral segregation processes as described above.

Crystalline minerals control stable Sr isotope fractionation during fractional crystallization. The main minerals for the Huili granites include quartz, plagioclase, K-feldspar, and micas. Since the Sr content in quartz is generally low (Rossman et al. 1987), the effect of quartz crystallization on $\delta^{88/86}Sr$ is likely to be negligible. In the granitic magmatic system, Sr is incompatible in biotite and muscovite (Icenhower and London 1995), and compatible in K-feldspar and plagioclase (Blundy and Wood 1991; Icenhower and London 1996), which is consistent with the Sr distribution in the minerals of the Huili granites (Fig. S5). Considering the limited proportions of biotite and muscovite in the crystalline mineral assemblage and the low Sr contents in the micas, we attribute the variation in $\delta^{88/86}Sr$ to the crystallization of feldspar rather than mica.

However, Sr isotopes behave differently during the crystallization of K-feldspar and plagioclase. For the two groups of the K-feldspar granites, the $\delta^{88/86}Sr$ values of the nine K-feldspar samples are slightly lower than those of the whole-rock samples with $\Delta^{88/86}Sr_{Kfs\text{-}WR}$ ranging from − 0.01‰ to − 0.13‰ (Fig. 3; Table S1), indicating

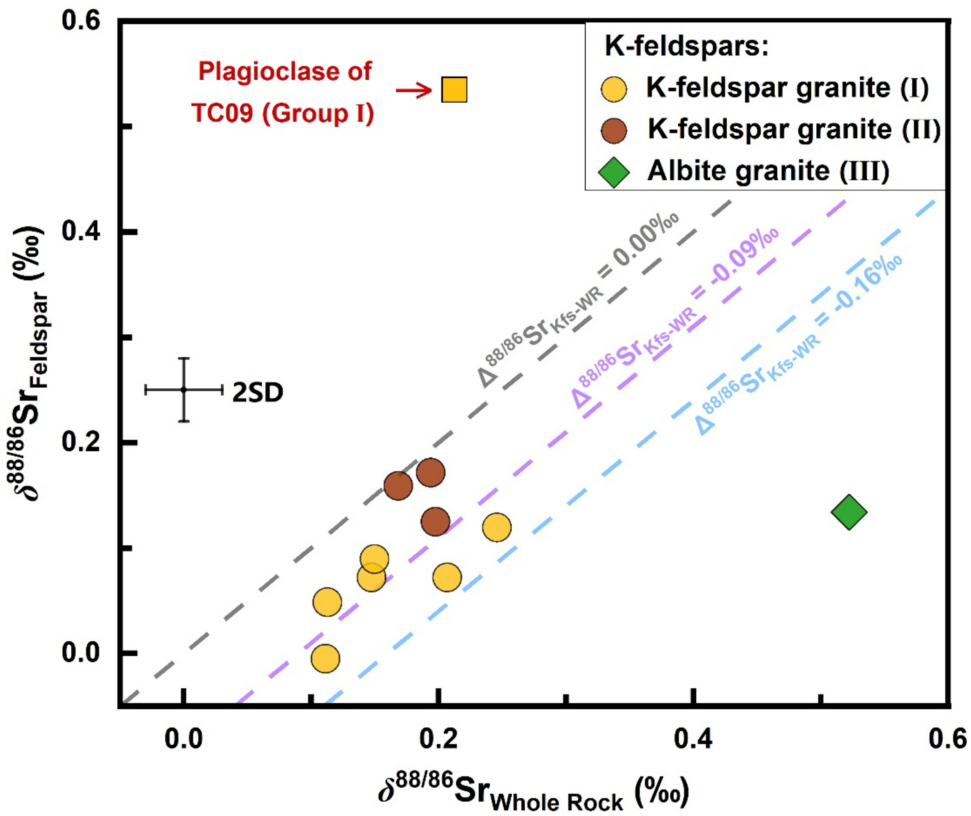

Fig. 3 The stable Sr isotopic compositions of whole rock and feldspars of Huili granites. The error bars represent two standard deviations based on the long-term external precision for $\delta^{88/86}Sr$ (2SD = ±0.03‰). The dashed lines have slopes of 1 and intercepts ($\delta^{88/86}Sr_{Feldspar} - \delta^{88/86}Sr_{Whole\ rock}$) of 0, −0.09‰, and −0.16‰, respectively. Acronym: Kfs: K-feldspar; WR: whole rock

that the K-feldspar is slightly enriched in light Sr isotopes relative to the melt during crystallization. In contrast, plagioclase may preferentially incorporate heavy Sr isotopes relative to the melt (Charlier et al. 2012), which is also supported by the $\delta^{88/86}Sr$ value of plagioclase measured in this study ($\Delta^{88/86}Sr_{Pl\text{-}WR} = +0.32$‰; Fig. 3; Table S1). The general formula of feldspar is MT_4O_8, where the M site hosts larger cations such as alkalis, alkaline earths, and other transition metals, and the T site hosts IV-fold coordinated smaller cations such as Si^{4+} and Al^{3+}. For K-feldspar, the M site contains cations in X-fold coordination with ideal ionic radius = 1.462–1.468 Å, which is larger than the ionic radius of Sr (1.36 Å, X-fold coordination) (Shannon et al. 1976; Arzilli et al. 2018). For plagioclase, the M site contains cations in VII to IX-fold coordination. The ionic radii of Sr in VII–IX-fold coordination (1.21–1.31 Å) are smaller than that in X-fold coordination (Shannon et al. 1976; Sun et al. 2017). Therefore, the different Sr isotopes fractionation behaviors of K-feldspar and plagioclase may due to the different coordinate environment, and the $\delta^{88/86}Sr$ of the interstitial melt may reflect the comprehensive contributions from K-feldspar and plagioclase during fractional crystallization of granitic magma.

During the magma differentiation of the Huili granites, K-feldspar crystallization controls the variation in $\delta^{88/86}Sr$. Previous study suggested that the 1.86 Ga Huili granites was derived from the remelting of 2.7–2.8 Ga ancient crust (Li et al. 2017), and the negative Eu anomalies (Eu/Eu* = 0.22–0.39; Li et al. 2017) of the Huili granites may be inherited from the magma source. The lack of correlation between $\delta^{88/86}Sr$ and Eu/Eu* also suggests that plagioclase cannot be the main cause for stable Sr isotopic fractionation (Fig. 2d). For the K-feldspar granites, the Sr content of plagioclase is similar to that of whole rock, and the Sr contents of K-feldspars (mineral proportion ~ 40%) are generally 2–3 times that of the relative whole rocks (Deng et al. 2021; Fig. S5). This indicates that early crystalized K-feldspar accumulated most of Sr, resulting in significant decrease of Sr content of the melt observed in the group III albite granite (Fig. S2). Since K-feldspar is slightly enriched in light Sr isotopes, its crystallization should also drive the residual melt toward an isotopically heavy composition, which can account for the high $\delta^{88/86}Sr$ values of group III albite granite. For the two groups of K-feldspar granites, since K-feldspar contributes most of the Sr budget, the whole-rock $\delta^{88/86}Sr$ is slightly different from that of K-feldspar. The $\delta^{88/86}Sr$ value of the K-feldspar in group III albite granite sample TC19 (0.13‰) is similar to the K-feldspars in the K-feldspar granites, which is likely to be the early crystallized K-feldspar carried by the extracted melt.

To better understand the behavior of Sr isotopes, we estimate the apparent Sr isotope fractionation factor using Rayleigh fractionation calculations to simulate the $\delta^{88/86}Sr$ during fractional crystallization (see Supplementary Materials

for details). The results show that when using group II K-feldspar granite to represent the residual crystal mush and assuming the extracted melt fraction $f_{ex}=0.3$, the high $\delta^{88/86}Sr$ values of group III albite granite can be explained by the Rayleigh model where $\Delta^{88/86}Sr_{solid\text{-}melt}$ ranges from −0.09‰ to −0.16‰ (Fig. 4). When using group I K-feldspar granite to represent the residual crystal mush, the $\Delta^{88/86}Sr_{solid\text{-}melt}$ becomes lower than −0.16‰, and this trend is consistent with the results that the $\Delta^{88/86}Sr_{Kfs\text{-}WR}$ of group I (−0.13‰ to −0.06‰) is lower than that of group II (−0.07‰ to −0.01‰) (Fig. 4).

4.3 Combining stable Sr and Ba isotopes to trace magmatism

Sr and Ba are both alkaline earth metal elements with similar geochemical properties during magmatism. The stable Sr and Ba isotopic compositions of the Huili granites show a nice positive correlation ($R^2=0.94$; Fig. 5), which may be due to the similar element partitioning and isotope fractionation behaviors of Sr and Ba between the main crystalline mineral (i.e., K-feldspar) and residual melt. K-feldspar is more enriched in Sr and Ba (Fig. S5) and light isotopes compared to the residual melt (Deng et al. 2021; Sect. 4.2), and crystalline K-feldspar results in significantly lower Sr and Ba contents and heavier Sr and Ba isotopic compositions of the residual melt. The variation of $\delta^{88/86}Sr$ is relatively smaller than $\delta^{138/134}Ba$ because of the different isotope fractionation factors between K-feldspar and granitic melt (Deng et al. 2021; Sect. 4.2). Similar coupling of the two isotope systems are also observed in Fe-V isotopes of alkali basalts (Chen et al. 2023) and Mg-Zn isotopes of basalts from eastern China (Liu et al. 2016), where the related elements are controlled by same phases. As the coexisting minerals showed

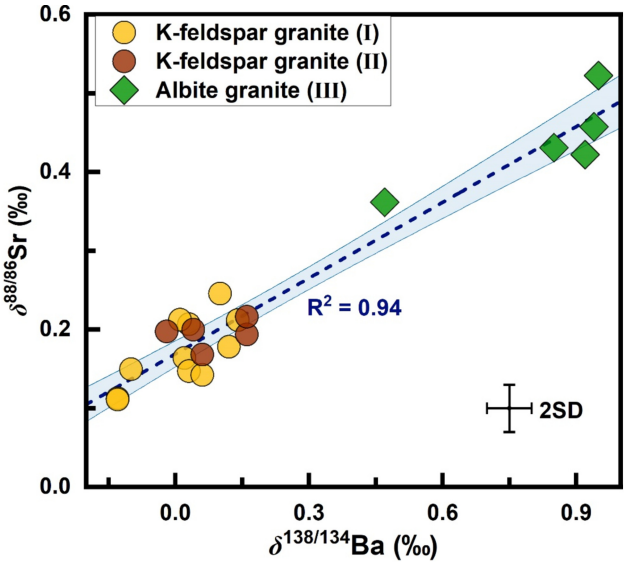

Fig. 5 Correlations of whole-rock stable Sr and Ba isotopic compositions (Deng et al. 2021) of Huili granites. The blue shade represents the 95% confidence interval. The error bars represent two standard deviations based on the long-term external precisions for $\delta^{88/86}Sr$ (2SD = ±0.03‰) and $\delta^{138/134}Ba$ (2SD = ±0.05‰)

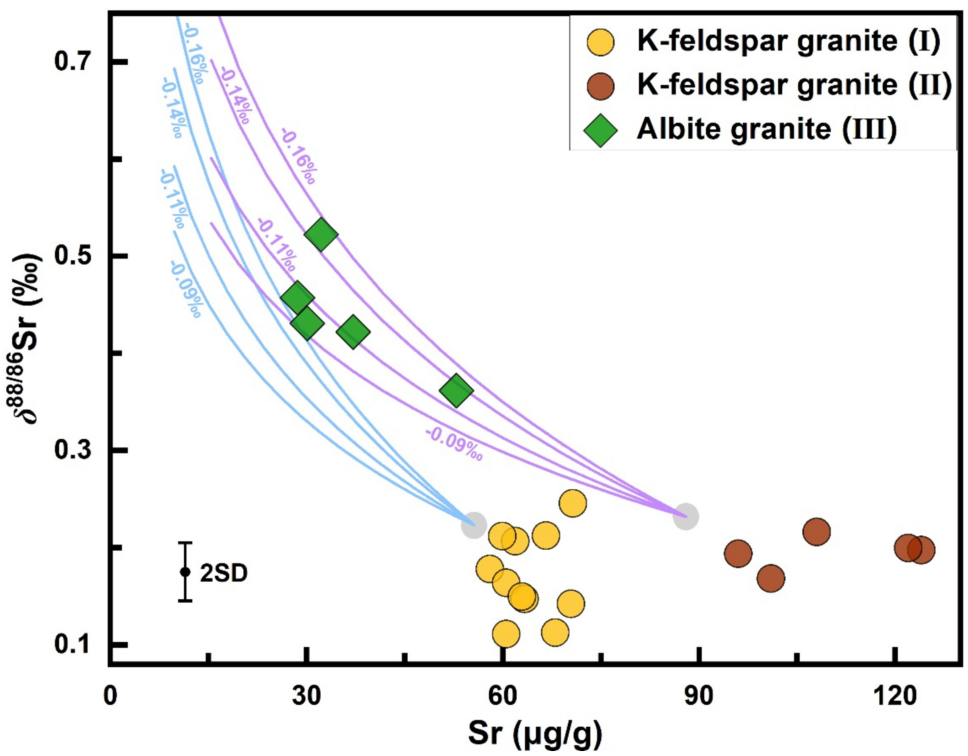

Fig. 4 Rayleigh fractionation models for stable Sr isotope evolution of residual melt during fractional crystallization of K-rich magma. A constant bulk fractionation factor between solid and melt ($\alpha_{solid\text{-}melt}$) and $f_{ex}=0.3$ are assumed. The initial Sr isotopic compositions (grey circles) are calculated using the mass balance equations. Curves stand for different bulk fractionation factors (curve labels = $\Delta^{88/86}Sr_{solid\text{-}melt} \sim 10^3 ln\alpha_{solid\text{-}melt}$). Calculations are detailed in the Supplementary Materials. The error bar represents two standard deviations based on the long-term external precision for $\delta^{88/86}Sr$ (2SD = ±0.03‰)

Ba isotope disequilibrium signatures (Deng et al. 2021), the $\delta^{88/86}$Sr of the Huili granites may also reflect the result of crystal repacking during crystal-melt separation.

We can further predict that $\delta^{88/86}$Sr and $\delta^{138/134}$Ba may be decoupled if crystallization is dominated by other minerals, such as plagioclase, another important mineral in granitic magma differentiation. Because plagioclase is compatible for Sr (Blundy and Wood 1991) and likely enriched in heavy Sr isotopes (Charlier et al. 2012), its crystallization should result in low Sr content and light Sr isotopic composition of the residual melt. In contrast, as Ba is incompatible or less compatible in plagioclase (e.g., Sun et al. 2017), the crystallization of plagioclase less likely affects Ba content and Ba isotopic composition of the residual melt. Although further study is needed on the relationship between $\delta^{88/86}$Sr and $\delta^{138/134}$Ba, the coupling and decoupling of Sr and Ba isotopes may reveal the controlling of different minerals during fractional crystallization.

5 Conclusions

We report stable Sr isotope data for the Huili granites to investigate the behaviors of Sr isotopes during crystal-melt separation in granitic magmatic system. During the K-feldspar-dominating crystal-melt separation for the Huili granites, K-feldspar is slightly enriched in light Sr isotopes, leading to a heavy Sr isotopic composition of the residual melt. Since K-feldspar contributes most of the Sr budget, extraction of the interstitial melt does not obviously deviate the residual crystal mush from the initial $\delta^{88/86}$Sr, but the extracted Na-rich interstitial melt which represented by the group III albite granite has significantly higher $\delta^{88/86}$Sr values (0.36‰–0.52‰) than the K-feldspar granite (0.11‰–0.25‰). The $\delta^{88/86}$Sr and $\delta^{138/134}$Ba of the Huili granites exhibit highly consistent variation toward the isotopically heavy direction, indicating the similar element partitioning and isotope fractionation behaviors during K-feldspar crystallization. The combination of stable Sr and Ba isotopes may give us new constraints on granitic magmatism.

Acknowledgements We are grateful to Youlian Li and Jinghui Guo for providing samples and stimulating discussions. This work was financially supported by National Natural Science Foundation of China (42473009).

Author contributions Xuqi Chen: Methodology, formal analysis, investigation, writing—original draft. Gengxin Deng: Investigation, writing—review and editing. Dingsheng Jiang: Writing—review and editing. Xiaoyun Nan: Funding acquisition. Fang Huang: conceptualization, resources, writing—review and editing, project administration, funding acquisition.

Data availability Data are available through Mendeley Data at https://doi.org/10.17632/k34hhxfb5p.2.

Declarations

Conflict of interest On behalf of all authors, the corresponding author states that there is no conflict of interest.

References

Amsellem E, Moynier F, Day JMD, Moreira M, Puchtel IS, Teng FZ (2018) The stable strontium isotopic composition of ocean island basalts, mid-ocean ridge basalts, and komatiites. Chem Geol 483:595–602. https://doi.org/10.1016/j.chemgeo.2018.03.030

Andrews MG, Jacobson AD (2017) The radiogenic and stable Sr isotope geochemistry of basalt weathering in Iceland: role of hydrothermal calcite and implications for long-term climate regulation. Geochim Cosmochim Acta 215:247–262. https://doi.org/10.1016/j.gca.2017.08.012

Andrews MG, Jacobson AD, Lehn GO, Horton TW, Craw D (2016) Radiogenic and stable Sr isotope ratios (^{87}Sr/^{86}Sr, $\delta^{88/86}$Sr) as tracers of riverine cation sources and biogeochemical cycling in the Milford sound region of Fiordland, New Zealand. Geochim Cosmochim Acta 173:284–303. https://doi.org/10.1016/j.gca.2015.10.005

Arzilli F, Fabbrizio A, Schmidt MW, Petrelli M, Maimaiti M, Dingwell DB, Paris E, Burton M, Carroll MR (2018) The effect of diffusive re-equilibration time on trace element partitioning between alkali feldspar and trachytic melts. Chem Geol 495:50–66. https://doi.org/10.1016/j.chemgeo.2018.07.035

Bachmann O, Huber C (2016) Silicic magma reservoirs in the Earth's crust. Am Mineral 101:2377–2404. https://doi.org/10.2138/am-2016-5675

Ballouard C, Poujol M, Boulvais P, Branquet Y, Tartèse R, Vigneresse JL (2016) Nb-Ta fractionation in peraluminous granites: A marker of the magmatic-hydrothermal transition. Geology 44:231–234. https://doi.org/10.1130/G37475.1

Bau M (1996) Controls on the fractionation of isovalent trace elements in magmatic and aqueous systems: evidence from Y/Ho, Zr/Hf, and lanthanide tetrad effect. Contrib Miner Petrol 123:323–333. https://doi.org/10.1007/s004100050159

Bekaert DV, Auro M, Shollenberger QR, Liu MC, Marschall H, Burton KW, Jacobsen B, Brennecka GA, MacPherson GJ, von Mutius R, Sarafian A, Nielsen SG (2021) Fossil records of early solar irradiation and cosmolocation of the CAI factory: A reappraisal. Sci Adv 7:eabg8329. https://doi.org/10.1126/sciadv.abg8329

Blundy JD, Wood BJ (1991) Crystal-chemical controls on the partitioning of Sr and Ba between plagioclase feldspar, silicate melts, and hydrothermal solutions. Geochim Cosmochim Acta 55:193–209. https://doi.org/10.1016/0016-7037(91)90411-W

Charlier BLA, Nowell GM, Parkinson IJ, Kelley SP, Pearson DG, Burton KW (2012) High temperature strontium stable isotope behaviour in the early solar system and planetary bodies. Earth Planet Sci Lett 329–330:31–40. https://doi.org/10.1016/j.epsl.2012.02.008

Charlier BLA, Parkinson IJ, Burton KW, Grady MM, Wilson CJN, Smith EGC (2017) Stable strontium isotopic heterogeneity in the solar system from double-spike data. Geochem Persp Let 4:35–40. https://doi.org/10.7185/geochemlet.1733

Chen XQ, Zeng Z, Yu HM, Sun N, Huang F (2022) Precise measurements of $\delta^{88/86}$Sr for twenty geological reference materials by double-spike MC-ICP-MS. Int J Mass Spectrom 479:116883. https://doi.org/10.1016/j.ijms.2022.116883

Chen Z, Ding X, Kiseeva ES, Lin X, Huang J, Huang F (2023) Vanadium isotope fractionation of alkali basalts during mantle melting. Lithos 442–443:107082. https://doi.org/10.1016/j.lithos.2023.107082

Deng G, Kang J, Nan X, Li Y, Guo J, Ding X, Huang F (2021) Barium isotope evidence for crystal-melt separation in granitic magma reservoirs. Geochim Cosmochim Acta 292:115–129. https://doi.org/10.1016/j.gca.2020.09.027

Fan JJ, Wang Q, Ma L, Li J, Zhang XZ, Zhang L, Wang ZL (2022) Extreme Mo isotope variations recorded in high-SiO_2 granites: Insights into magmatic differentiation and melt-fluid interaction. Geochim Cosmochim Acta 334:241–258. https://doi.org/10.1016/j.gca.2022.08.009

Faure G (1986) Principles of isotope geology, 2nd edn. John Wiley and Sons, New York.

Hofmann AW (1988) Chemical differentiation of the Earth: the relationship between mantle, continental crust, and oceanic crust. Earth Planet Sci Lett 90:297–314. https://doi.org/10.1016/0012-821X(88)90132-X

Icenhower J, London D (1995) An experimental study of element partitioning among biotite, muscovite, and coexisting peraluminous silicic melt at 200 MPa (H_2O). Am Mineral 80:1229–1251. https://doi.org/10.2138/am-1995-11-1213

Icenhower J, London D (1996) Experimental partitioning of Rb, Cs, Sr, and Ba between alkali feldspar and peraluminous melt. Am Miner 81:719–734. https://doi.org/10.2138/am-1996-5-619

Iveson AA, Webster JD, Rowe MC, Neill OK (2019) Fluid-melt trace-element partitioning behaviour between evolved melts and aqueous fluids: experimental constraints on the magmatic-hydrothermal transport of metals. Chem Geol 516:18–41. https://doi.org/10.1016/j.chemgeo.2019.03.029

Keppler H (2017) Fluids and trace element transport in subduction zones. Am Miner 102:5–20. https://doi.org/10.2138/am-2017-5716

Klaver M, Lewis J, Parkinson IJ, Elburg MA, Vroon PZ, Kelley KA, Elliott T (2020) Sr isotopes in arcs revisited: tracking slab dehydration using $\delta^{88/86}Sr$ and $^{87}Sr/^{86}Sr$ systematics of arc lavas. Geochim Cosmochim Acta. https://doi.org/10.1016/j.gca.2020.08.010

Li Y, Zhang H, Guo J, Li C (2017) Petrogenesis of the Huili Paleoproterozoic leucogranite in the Jiaobei Terrane of the North China Craton: a highly fractionated albite granite forced by K-feldspar fractionation. Chem Geol 450:165–182. https://doi.org/10.1016/j.chemgeo.2016.12.029

Liu HC, You CF, Huang KF, Chung CH (2012) Precise determination of triple Sr isotopes ($\delta^{87}Sr$ and $\delta^{88}Sr$) using MC-ICP-MS. Talanta 88:338–344. https://doi.org/10.1016/j.talanta.2011.10.050

Liu SA, Wang ZZ, Li SG, Huang J, Yang W (2016) Zinc isotope evidence for a large-scale carbonated mantle beneath eastern China. Earth Planet Sci Lett 444:169–178. https://doi.org/10.1016/j.epsl.2016.03.051

Meija J, Coplen TB, Berglund M, Brand WA, De Bièvre P, Gröning M, Holden NE, Irrgeher J, Loss RD, Walczyk T, Prohaska T (2016) Isotopic compositions of the elements 2013 (IUPAC Technical Report). Pure Appl Chem 88:293–306. https://doi.org/10.1515/pac-2015-0503

Michaud JAS, Pichavant M (2020) Magmatic fractionation and the magmatic-hydrothermal transition in rare metal granites: evidence from Argemela (Central Portugal). Geochim Cosmochim Acta 289:130–157. https://doi.org/10.1016/j.gca.2020.08.022

Moynier F, Agranier A, Hezel DC, Bouvier A (2010) Sr stable isotope composition of earth, the moon, mars, vesta and meteorites. Earth Planet Sci Lett 300:359–366. https://doi.org/10.1016/j.epsl.2010.10.017

Nesbitt HW, Young GM (1982) Early Proterozoic climates and plate motions inferred from major element chemistry of lutites. Nature 299:715–717. https://doi.org/10.1038/299715a0

Nier AO (1938) The isotopic constitution of strontium, barium, bismuth, thallium and mercury. Phys Rev 54:275–278. https://doi.org/10.1103/PhysRev.54.275

Ohno T, Komiya T, Ueno Y, Hirata T, Maruyama S (2008) Determination of $^{88}Sr/^{86}Sr$ mass-dependent isotopic fractionation and radiogenic isotope variation of $^{87}Sr/^{86}Sr$ in the neoproterozoic doushantuo formation. Gondwana Res 14:126–133. https://doi.org/10.1016/j.gr.2007.10.007

Paytan A, Griffith EM, Eisenhauer A, Hain MP, Wallmann K, Ridgwell A (2021) A 35-million-year record of seawater stable Sr isotopes reveals a fluctuating global carbon cycle. Science 371:1346–1350. https://doi.org/10.1126/science.aaz9266

Prowatke S, Klemme S (2006) Trace element partitioning between apatite and silicate melts. Geochim Cosmochim Acta 70:4513–4527. https://doi.org/10.1016/j.gca.2006.06.162

Rossman GR, Weis D, Wasserburg GJ (1987) Rb, Sr, Nd and Sm concentrations in quartz. Geochim Cosmochim Acta 51:2325–2329. https://doi.org/10.1016/0016-7037(87)90286-9

Rudnick RL, Fountain DM (1995) Nature and composition of the continental crust: a lower crustal perspective. Rev Geophys 33:267–309. https://doi.org/10.1029/95RG01302

Shannon RD (1976) Revised effective ionic radii and systematic studies of interatomic distances in halides and chalcogenides. Acta Crystallogr Sect A 32:751–767. https://doi.org/10.1107/S0567739476001551

Shao Y, Farkaš J, Mosley L, Tyler J, Wong H, Chamberlayne B, Raven M, Samanta M, Holmden C, Gillanders BM, Kolevica A, Eisenhauer A (2021) Impact of salinity and carbonate saturation on stable Sr isotopes ($\delta^{88/86}Sr$) in a lagoon-estuarine system. Geochim Cosmochim Acta 293:461–476. https://doi.org/10.1016/j.gca.2020.11.014

Sun C, Craff M, Liang Y (2017) Trace element partitioning between plagioclase and silicate melt: the importance of temperature and plagioclase composition, with implications for terrestrial and lunar magmatism. Geochim Cosmochim Acta 206:273–295. https://doi.org/10.1016/j.gca.2017.03.003